Maria E. Schweinefuß, Sergej Springer, Igor A. Baburin, Todor Hikov, Klaus Huber, Stefano Leoni, Michael Wiebcke

Zeolitic imidazolate framework-71 nanocrystals and a novel SOD-type polymorph: solution mediated phase transformations, phase selection via coordination modulation and a density functional theory derived energy landscape

Erstveröffentlichung in / First published in:

Dalton Transactions. 2014, 43(9), S. 3528–3536 [Zugriff am: 01.11.2019]. Royal Society of Chemistry. ISSN 1364-5447.

DOI: https://doi.org/10.1039/c3dt52992d

Dalton Transactions

PAPER

View Article Online
View Journal | View Issue

Cite this: *Dalton Trans.*, 2014, **43**, 3528

Zeolitic imidazolate framework-71 nanocrystals and a novel SOD-type polymorph: solution mediated phase transformations, phase selection *via* coordination modulation and a density functional theory derived energy landscape†

Maria E. Schweinefuß,[a] Sergej Springer,[a] Igor A. Baburin,[b] Todor Hikov,[c] Klaus Huber,[c] Stefano Leoni*[b,d] and Michael Wiebcke*[a]

Received 23rd October 2013,
Accepted 16th December 2013

DOI: 10.1039/c3dt52992d

www.rsc.org/dalton

We report a rapid additive-free synthesis of nanocrystals (NCs) of RHO-type ZIF-71 (**1**) of composition [Zn(dcim)$_2$] (dcim = 4,5-dichloroimidazolate) in 1-propanol as solvent at room temperature. NC-**1** has a size of 30–60 nm and exhibits permanent microporosity with a surface area (S_{BET} = 970 m^2 g^{-1}) comparable to that of microcrystalline material. When kept under the mother solution NC-**1** undergoes transformation into a novel SOD-type polymorph (**2**), which in turn converts into known ZIF-72 (**3**) with lcs topology. It is shown that microcrystals (MCs) of **2** can be favourably synthesised using 1-methylimidazole as a coordination modulator. NC-**2** with size <200 nm was prepared using NC-ZIF-8 as a template with SOD topology in a solvent assisted ligand exchange-related process. DFT-assisted Rietveld analysis of powder XRD data revealed that novel polymorph **2** possesses an unusual SOD framework conformation. **2** was further characterised with regard to microporosity (S_{BET} = 597 m^2 g^{-1}) and thermal as well as chemical stability. DFT calculations were performed to search for further potentially existing but not-yet synthesised polymorphs in the [Zn(dcim)$_2$] system.

Introduction

Crystalline porous zeolitic imidazolate frameworks (ZIFs) are assembled from tetrahedrally coordinating divalent metal cations and bridging ditopic imidazolate anions and possess zeolite-related frameworks with about 30 different topologies known so far. Additional chemical diversity results from various substituents at the imidazolate linker.[1] Some ZIFs are reported to exhibit high thermal and chemical stability.[2] Therefore, ZIFs are currently attracting considerable attention for many potential applications in gas storage,[3] separation,[4] catalysis[5] and increasing numbers of other fields.[6]

With applications in mind the development of synthetic methods that allow tuning of crystal size and shape on the nano- and microscale is currently a focus of interest.[7,8] Since the potential existence of not-yet-synthesised ZIFs is anticipated[1a] and has been theoretically predicted,[9] another important aspect is the further development of syntheses with respect to methodology[10,11] as well as a mechanistic understanding of the crystallisation processes.[12]

With Zn^{2+} centres and the 4,5-dichloroimidazolate (dcim) linker two ZIF polymorphs, microporous RHO-type ZIF-71[3,13] (**1**) and essentially non-porous lcs-type ZIF-72[3] (**3**), have so far been synthesised. Theory[14] and experiments[15] have shown that **1** is hydrophobic with promising characteristics for separation of organics–water mixtures. In addition, supported membranes of intergrown **1** crystals and mixed matrix membranes containing MC-**1** particles have been recently fabricated and successfully used for pervaporation separations of liquid alcohol–water and dimethyl carbonate–methanol mixtures.[16]

[a]*Institut für Anorganische Chemie, Leibniz Universität Hannover, Callinstrasse 9, 30167 Hannover, Germany. E-mail: Michael.Wiebcke@acb.uni-hannover.de; Fax: +49 511 7623006; Tel: +49 511 7623698*
[b]*Institut für Physikalische Chemie und Elektrochemie, Technische Universität Dresden, Mommsenstrasse 13, 01062 Dresden, Germany*
[c]*Department Chemie, Universität Paderborn, Warburger Strasse 100, 33098 Paderborn, Germany*
[d]*School of Chemistry, Cardiff University, Main Building, Park Place, Cardiff, CF10 3AT, UK. E-mail: Leoni@cardiff.ac.uk; Fax: +44 (0)29 20874030; Tel: +44 (0)29 20875856*

†Electronic supplementary information (ESI) available: XRD patterns, TG/DTA traces, VT-XRD patterns, SEM images for NC-**1** and **2**; Rietveld plots and structural data (including CIF file) for **2**; DFT-optimsed hypothetical ZIF network structures (CIF file). See DOI: 10.1039/c3dt52992d

Following our previous work on NC-ZIF-8[7a] we here report a rapid room-temperature and additive-free synthesis of NC-**1**. In the course of this work we discovered a sequence of solution mediated phase transformations, the conversion of NC-**1** into a novel ZIF (**2**) with SOD framework topology and the subsequent conversion of **2** into **3**. In seeking to improve the crystallinity of **2** we explored the coordination modulation[7c,17] and recently reported solvent assisted ligand exchange[11] methods. Since the obtained single crystals of **2** were poorly diffracting and had a complex internal architecture, first structure analysis had to rely on powder X-ray diffraction (XRD) data. Thermal and chemical stability as well as microporosity of NC-**1** and novel polymorph **2** were investigated employing thermogravimetric (TG) analysis, variable-temperature (VT) XRD and Ar physisorption measurements. Furthermore, density functional theory (DFT) calculations were performed to support structure analysis of **2**, theoretically investigate the relative stabilities of polymorphs **1**–**3** and search for potentially existing but not-yet synthesised polymorphs in the [Zn(dcim)$_2$] system as further synthetic targets.

Results and discussion

Synthesis and characterisation of NC-1

Following our previous work on the synthesis of NC-ZIF-8[7a] we were able to prepare NC-**1** simply by combining 1-propanolic solutions of $Zn(NO_3)_2{\cdot}6H_2O$ and Hdcim followed by work up after 10 min. Using more polar methanol as a solvent as in the previous work only MC-**1** was obtained under similar conditions (Fig. S1†).

SEM images reveal that NC-**1** consists of spherical particles with a diameter of 30–60 nm that are pure phase RHO-type material as demonstrated by powder XRD patterns (Fig. 1). Our NC-**1** particles are significantly smaller in size than previously reported ones (>several 100 nm).[15a,16a] In TG traces measured in flowing air (Fig. S2†) only a small gradual mass loss of 3.7% occurs up to *ca.* 320 °C possibly originating from some residual unreacted Hdcim. Subsequent large mass losses (90.8% in total) indicate framework decomposition. The final product is ZnO according to XRD. The latter mass losses are larger than calculated for the removal of dcim (75.9%) meaning that some (unknown) volatile Zn species escape at high temperatures above 700 °C in addition to the dcim moiety (*e.g.* the boiling point of $ZnCl_2$ is 732 °C). The good thermal stability of NC-**1** in air is confirmed by VT-XRD patterns (Fig. S3†). These patterns reveal that the RHO framework is stable up to *ca.* 250 °C (decrease of reflection intensities starts above *ca.* 150 °C).

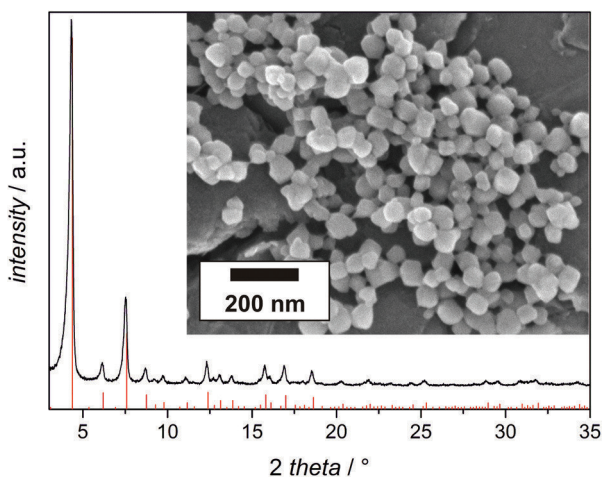

Fig. 1 NC-**1**: SEM image (inset) and experimental (black profile) and simulated XRD pattern (red bars).

According to Ar adsorption–desorption isotherms measured at −186 °C (Fig. S4†) NC-**1** exhibits microporosity with a Brunauer–Emmett–Teller (BET) surface area of 970 m^2 g^{-1} and a micropore volume of 0.36 cm^3 g^{-1} (taken at p/p_0 = 0.13, corresponding to d_{pore} < 2 nm). Hence the total surface area of our NC-**1** is as large as that reported previously for microcrystalline material (964–1186 m^2 g^{-1}).[11b,15a] Chemical stability was tested by keeping as-prepared NC-**1** in various alcohols (MeOH, EtOH, and 1-PrOH) and deionised water at room temperature for one week. Subsequently recorded XRD patterns indicate no change in the cases of alcohols but partial transformation of NC-**1** into lcs-type **3** in water (Fig. S5†). The latter observation may hint at potential problems in long term applications of **1** under aqueous or humid conditions.

Solution mediated phase transformations

When NC-**1** was kept under the mother solution at room temperature for a longer time it transformed into the novel SOD-type polymorph **2**. This was first observed for some (but not all) experiments in SEM images taken after 1 h of aging which show besides the large number of small NC-**1** particles some considerably bigger crystals with a rhombic dodecahedral shape (Fig. 2a) which can be assigned to **2**. The minor fraction of **2** is not revealed in accompanying XRD measurements. After 24 h well shaped crystals of **2** (a few μm in size) are seen besides NC-**1** in SEM images for all experiments (Fig. 2b) and additionally recorded XRD patterns indicate a mixture of **1** and **2** (Fig. 3). XRD patterns recorded in intervals of 1 d revealed that the transformation of NC-**1** into **2** was complete after 4 d and that **2** started to transform further into lcs-type **3** after 7 d (Fig. 3 and Fig. S6†). In SEM images after 7 d the crystals of **3** (a few μm in size) can be clearly identified by their distinct deltoidicositetrahedral shape (Fig. 2c). The complete conversion process of **2** into **3** was not further studied.

The observed solution mediated phase transformations suggest increasing thermodynamic stability of the phases in the order **1** < **2** < **3**. This order follows the densities of frameworks with RHO, SOD and lcs topology and is therefore as expected.[18] Similar solution mediated transformations have been reported previously for a few ZIFs containing the unsubstituted imidazolate (im) linker.[19] In addition, the conversion from RHO to SOD framework was reported recently for a Co-based ZIF with the 2-nitroimidazolate linker.[20] This indicates that solution mediated phase transformations may be a more

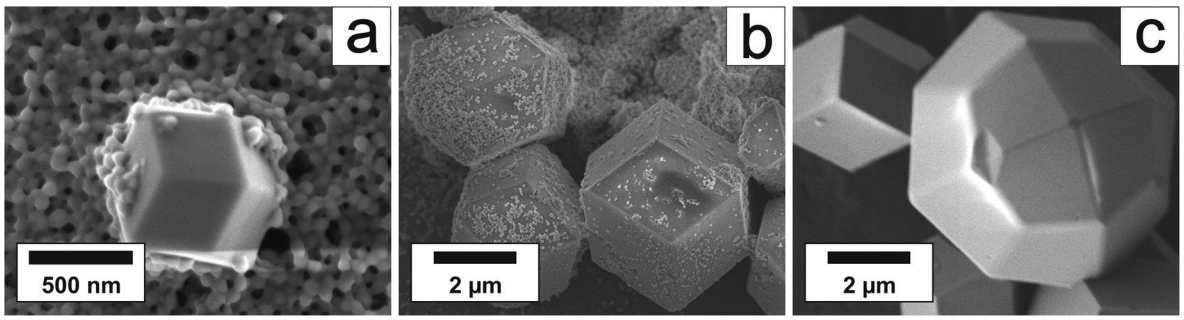

Fig. 2 SEM images taken at different time intervals during solution mediated transformations of NC-**1**: (a) 1 h; (b) 24 h; (c) 7 d, the deltoidicositetrahedral crystal in the foreground belongs to **3**, while the smaller rhombic dodecahedra in the background belong to **2**.

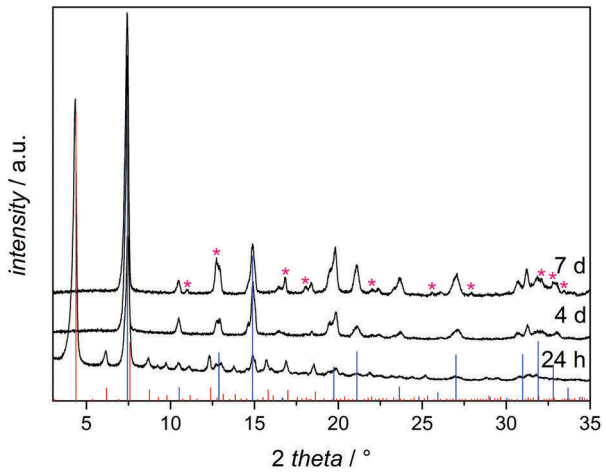

Fig. 3 Experimental XRD patterns (black profiles) recorded at different time intervals (as indicated) during solution mediated transformations of NC-**1**; patterns simulated from structural data of **1** (red bars) and cubic **2** (blue bars) are presented for comparison; the pink asterisks indicate reflections that belong to **3**.

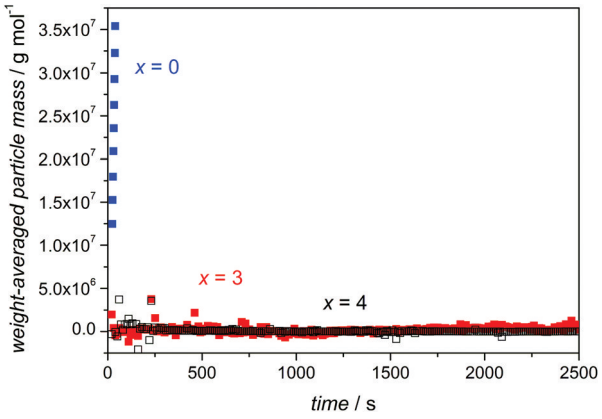

Fig. 4 Evolution of particle mass as a function of time for the syntheses with molar ratios of Zn/Hdcim/1-mim/1-PrOH = 1 : 4 : *x* : 1000, *x* values are indicated.

common phenomenon in ZIF systems and worth studying by time dependent experiments in order to improve our understanding of ZIF crystallisation.

The XRD patterns recorded from **2** obtained *via* solution mediated transformation of NC-**1** suggest a SOD-type framework structure. The comparison with a pattern simulated for a cubic SOD framework reveals that some reflections in the experimental pattern are split or exhibit a broad, asymmetric shape indicating a deviation from cubic symmetry (*e.g.* see the XRD pattern after 4 d in Fig. 3 and Fig. S6†). The crystallinity is rather poor (reflection intensities vanish already above *ca.* 38° 2θ) in spite of the well shaped MCs seen in SEM images (Fig. 2). We therefore attempted to improve crystallinity and to grow big crystals suitable for single crystal X-ray structure analysis.

Synthesis of 2 *via* coordination modulation

We first applied the coordination modulation method,[17] which is now widely used to tune crystal size and improve crystallinity, and introduced 1-methylimidazole (1-mim) into the synthesis mixtures of molar ratio Zn/Hdcim/1-mim/1-PrOH = 1 : 4 : *x* : 1000 (*x* = 1, 3, 4) at room temperature. Monodentate 1-mim can act both as a coordination modulator (in competition to bridging Hdcim) and as a deprotonation modulator (deprotonation of Zn–Hdcim complexes) in coupled coordination and acid–base equilibria.[7c,21] Time-resolved *in situ* static light scattering (SLS) experiments were performed. Fig. 4 shows the evolution of particle mass with time as extracted from the SLS data. In the non-modulated synthesis (*x* = 0) particle formation occurs nearly instantaneously and growth is very rapid, as expected since we can isolate NC-**1** already after 10 min. For *x* = 1 particle formation appeared to occur even more rapidly and could not be followed by SLS because of a rise in turbidity which was too rapid. At *x* = 3 and 4, however, particle formation is slowed down significantly and particles could not be detected by SLS during the first 40 min of the reaction. In these latter cases a coordination modulation function of 1-mim can be inferred due to the effective competition of 1-mim with Hdcim at the Zn centres. XRD patterns taken from the products of the 1-mim modulated syntheses at *x* = 1 after 10 min and 1 d both reveal the formation of pure phase RHO-type **1** (Fig. 5). Spherical NCs are seen in SEM images in both cases (Fig. S7a and S7b†) that are somewhat larger than those obtained by non-modulated synthesis (Fig. 1a). For *x* = 3 and 4 enough solid material to enable *ex situ* XRD measurements to

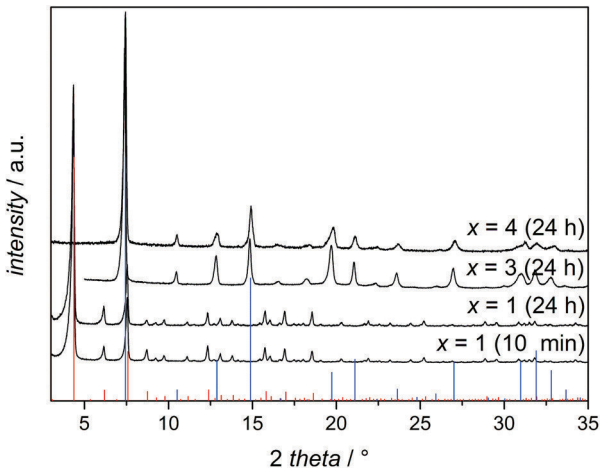

Fig. 5 XRD patterns recorded from products of modulated syntheses with molar ratios of Zn/Hdcim/1-mim/1-PrOH = 1 : 4 : *x* : 1000, *x* values and synthesis times are indicated; simulated XRD patterns of **1** (red bars) and cubic **2** (blue bars) are presented for comparison.

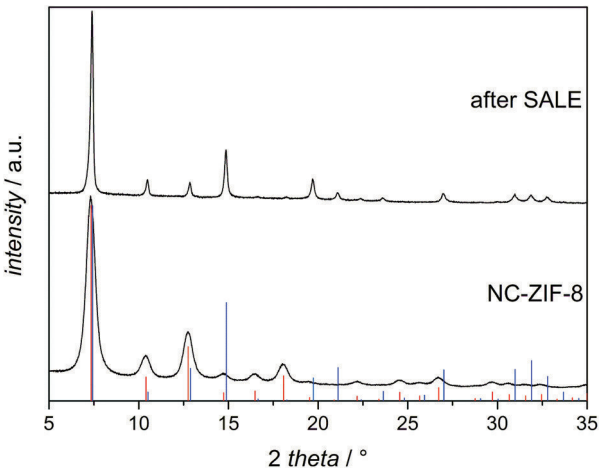

Fig. 6 XRD patterns of the NC-ZIF-8 template used for SALE and NC-**2** obtained after SALE; simulated XRD patterns of ZIF-8 (red bars) and cubic **2** (blue bars) are presented for comparison.

be performed could only be obtained after 1 d. These XRD patterns are consistent with pure phase SOD-type **2** (Fig. 5). In SEM images, strongly aggregated MCs with a rhombic dodecahedral shape are seen (Fig. S7c and S7d†). Thus, our *ex situ* studies indicate that under the latter conditions of high 1-mim concentrations (x = 3–4) **2** selectively crystallises directly from solution without prior formation of **1**. However, this hypothesis has still to be verified by *in situ* XRD investigations.

Product **2** obtained for x = 3 shows an XRD pattern (Fig. 5) that can be indexed on a body-centred cubic unit cell. However, some reflections are slightly broadened which may be taken as an indication of slight deviation from cubic symmetry. The material is rather poorly diffracting to high 2θ angles.

The parameters in the modulated syntheses could be further manipulated towards growth of bigger crystals, *e.g.* by increase of temperature up to 50 °C. At temperatures >50 °C ready conversion of **2** into more stable **3** becomes a significant problem when trying to prepare pure phase **2**. The crystals grown were up to 100 μm in size and had a rhombic dodecahedral shape. However, when inspected with an optical microscope under crossed polarisers they exhibit birefringence with no clear extinctions when being rotated in the light path and frequently reveal Maltese crosses in addition (Fig. S8†) suggesting a complex internal architecture (twins of non-cubic domains). Such crystals were only poorly diffracting on a single crystal X-ray diffractometer (even when using CuK_α radiation) and not suitable for accurate structure analysis.

Synthesis of 2 *via* a solvent assisted ligand exchange-related process

We then turned to solvent assisted ligand exchange (SALE; also called post-synthetic ligand exchange, PSLE).[11] As a template with SOD topology we choose ZIF-8 containing the 2-methylimidazolate (2-mim) linker.[2] In order to facilitate the exchange kinetics we used NC-ZIF-8 prepared at room temperature with a particle size <20 nm (see the XRD pattern in Fig. 6a and SEM image in Fig. S9a†) as a starting material.[7c] NC-ZIF-8 was kept in 1-propanolic Hdcim solutions at 100 °C. The Hdcim solution was refreshed every 24 h. The degree of ligand exchange was monitored by means of the liquid-state ^{1}H-NMR of acid digested samples. After 5 d of reaction a nearly full (*ca.* 99%) replacement of 2-mim by dcim is observed (Fig. S10†) and the obtained **2** shows XRD patterns that are fully consistent with a body-centered cubic unit cell of a SOD-type ZIF (Fig. 6b). According to SEM images the product consists of irregular particles with a size up to 200 nm (Fig. S9b†). This means that besides ligand exchange significant growth of crystallites had occurred likely due to Ostwald ripening at the comparatively high temperature.

In contrast to the modulated and non-modulated syntheses presented above, during SALE solution mediated transformation of **2** into **3** was not observed. Hence, SALE can be performed at higher temperatures (>50 °C) enabling the preparation of **2** with clean cubic symmetry. In addition, as demonstrated here for the first time, SALE is a possible approach to the preparation of nanocrystalline material when starting with a nanocrystalline template. It is noted that under conditions of solution mediated phase transformation and coordination modulation nucleation occurs at comparatively low levels of supersaturation favouring the formation of microcrystalline rather than nanocrystalline material.

Crystal structure analysis of 2

Our best cubic powder sample obtained by SALE was used for structure analysis. Desolvated **2** was obtained by activating as-synthesised **2** *in vacuo* at 50 °C. The XRD pattern was successfully indexed on a body-centered cubic unit cell and DFT calculations were utilised to generate structural models. Assuming SOD topology[22] the dcim linker was placed between two Zn centres and twisted about the Zn···Zn edge. This way, two

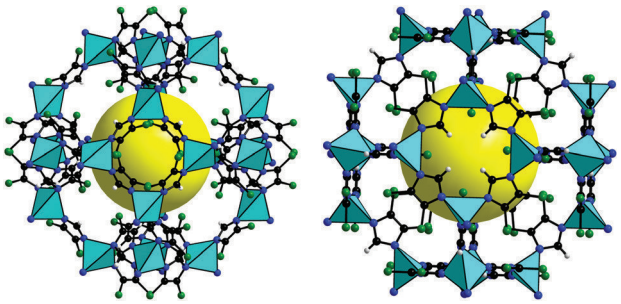

Fig. 7 Sodalite [$4^6{\cdot}6^8$] cages in frameworks **I** (left) and **II** (right); colour code: cyan, ZnN_4 tetrahedra; blue, N; black, C; green, Cl; white, H.

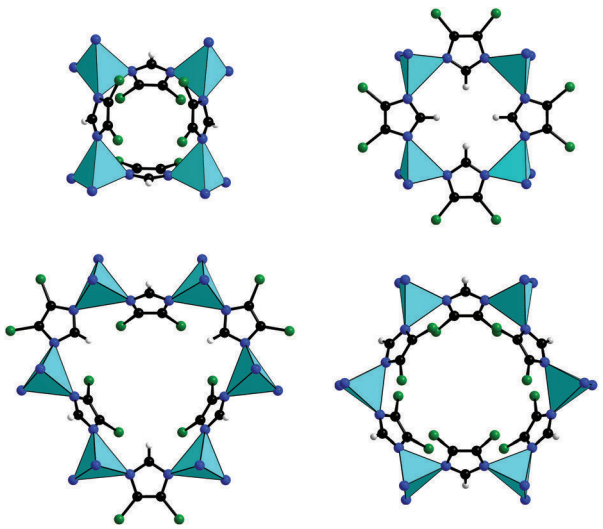

Fig. 8 4Rs and 6Rs in frameworks **I** (left) and **II** (right); colour code: cyan, ZnN_4 tetrahedra; blue, N; black, C; green, Cl; white, H.

reasonable framework conformations (**I** and **II** hereafter) were obtained that differ in total energy by 11.0 kJ mol^{-1} (at 0 K). The crystallographically independent sodalite [$4^6{\cdot}6^8$] cage as well as rings of four (4R) and six (6R) Zn–dcim–Zn bridges in frameworks **I** and **II** is compared in Fig. 7 and 8, respectively. The different ring conformations in both frameworks can be clearly seen. Framework **I** (space group $I\bar{4}3m$) represents the energy minimum and its conformation resembles those of other known cubic ZIFs which contain 2-substituted imidazolate linkers [ZIF-Me (ZIF-8), ZIF-CHO (ZIF-90), ZIF-Cl and ZIF-Br].[2,4b,23] Framework **II** (space group $Im\bar{3}m$) contains an unusual flat 4R in which the C–H vectors of the four dcim linkers point to the ring centre and is to the best of our knowledge unprecedented.

Interestingly, Rietveld refinements starting with the generated structures and allowing a twisting of the rigid dcim unit about a Zn···Zn edge (space group $I\bar{4}3m$) resulted in superior fits for framework **II** compared to **I**, suggesting that **2** crystallises with the higher energy framework **II**. The final Rietveld refinement plots for framework **II** are shown in Fig. 9 (see Fig. S11† for the Rietveld plots for framework **I**). The Rietveld fit is reasonable yet not completely satisfactory indicating that

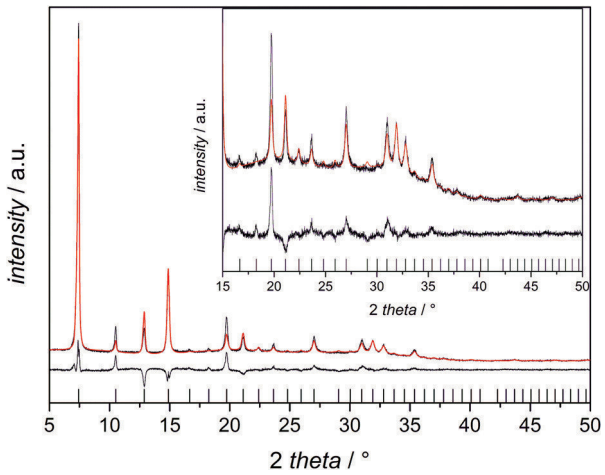

Fig. 9 Rietveld refinement plots for framework **II**; top: observed (black) and calculated (red) patterns; middle: difference plot; bottom: Bragg peak markers. For clarity, the inset shows an expanded view of the range 15–50° 2θ.

the structural model does not mirror all aspects in the real periodic structure possibly due to the slight, undetected deviation from cubic symmetry. Furthermore, the rather poor diffraction of the material to high 2θ values and the large displacement parameters obtained by Rietveld analysis for the Zn and linker atoms (the isotropic U values are 0.13 Å^2) are indicative of random local distortions from the structural model.

In framework **II** the Zn–N bond lengths (1.941 Å) and N–Zn–N bond angles (104.8–119.4°) fall in expected ranges. The planar aromatic dcim linker is slightly twisted (by −0.8°) out of the plane of a 4R defined by the four Zn centres (Fig. 10). The shortest inter-linker H···H (2.54 Å) and Cl···Cl distances (3.714 Å) are slightly larger than twice the van der Waals radius of hydrogen (1.2 Å) and chlorine (1.75 Å), respectively. The free diameters of the cage and the 6R window are estimated to be 8.6 and 3.2 Å, respectively, taking van der Waals radii into account. In comparison the larger [$4^{12}{\cdot}6^8{\cdot}8^6$] cage and 8R window in RHO-type **1** have free diameters of 16.5 and 4.2 Å, respectively.[3,13] A PLATON/SOLVE calculation[24] for

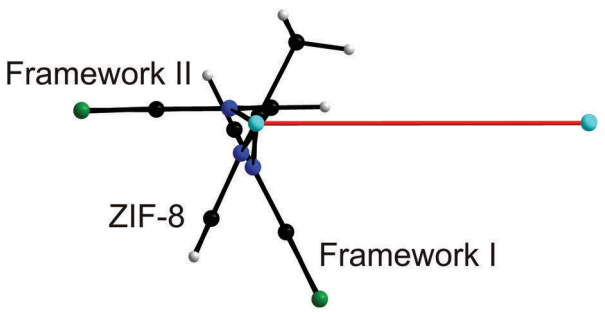

Fig. 10 Twist of the planar aromatic linkers out of the plane of a 4R defined by the four Zn atoms in framework **II**, ZIF-8 and framework **I**; the view is parallel to the linker and 4R (red line) planes; the twist angles are −0.8°, 65.2° and 116.7° for framework **II**, ZIF-8 and framework **I**, respectively; colour code: cyan, Zn; blue, N; black, C; green, Cl; white, H.

framework **II** yields a solvent accessible volume of 35.1% (probe radius 1.68 Å). Furthermore, we note that a cubic SOD-type polymorph is known for [Zn(fmim)$_2$] (fmim = 4-formyl-5-methylimidazolate; SIM-1)[25] with a reported cell parameter (a = 16.743 Å) similar to that of **2**. However, a detailed structure analysis is not yet available to the best of our knowledge.

The conformation of framework **II** deviates largely from the conformation of the SOD template ZIF-8 used in SALE (Fig. 10). This means that SALE transformation from the ZIF-8 framework to framework **II** is accompanied by considerable structural rearrangements. This process is possibly not a sole ligand exchange process but may include dissolution–recrystallisation steps (apart from the growth *via* Ostwald ripening mentioned above). A comparison of XRD patterns with simulated patterns indicates that independent of the synthetic method employed all our **2** products have structures resembling more of framework **II** than **I**. Structure analysis of the non-cubic variants of **2** is out of the scope of the present study.

Characterisation of 2

A detailed characterisation was performed using MC-**2** prepared by modulated synthesis. TG traces (Fig. S12†) exhibit an initial mass loss of 7.1% up to *ca.* 150 °C due to the escape of solvent molecules as confirmed by simultaneous mass spectrometric analysis (Fig. S13†). The mass losses (85.1% in total) at temperatures >300 °C indicate framework decomposition. These mass losses are larger than calculated for the dcim moiety (75.9%) probably due to the escape of some volatile Zn species as observed also for NC-**1**. VT-XRD patterns reveal changes in reflection intensities at *ca.* 150 °C at which temperature the solvent molecules have left the pore system according to TG (Fig. S14†). Those changes are most likely not only due to the loss of the guests but also due to some accompanying relaxation in the framework structure. The XRD pattern is re-established after keeping desolvated **2** in 1-PrOH, *i.e.* the changes are reversible. At *ca.* 250 °C desolvated **2** transforms into dense lcs-type **3** which in turn decomposes at *ca.* 320 °C. Thermally induced structural phase transitions in the solid state as the SOD-lcs transition observed here have rarely been reported for ZIFs before.[19c]

Activated **2** is microporous as can be seen from Ar adsorption–desorption isotherms measured at −186 °C (Fig. 11). The BET surface area and micropore volume amount to 597 m^2 g^{-1} and 0.23 cm^3 g^{-1} (taken at p/p_0 = 0.16), respectively. The latter value is in excellent agreement with the value calculated for the crystallographic solvent accessible volume (0.25 cm^3 g^{-1}). The adsorption–desorption hysteresis loop seen between 0.4 < p/p_0 < 0.8 indicates the presence of mesopores in line with the comparatively poor crystallinity of our products. Chemical stability was tested by keeping as-prepared **2** in various alcohols (MeOH, EtOH, and 1-PrOH) and deionised water for one week. According to subsequent XRD analyses **2** is stable in alcohols (Fig. S15†). In water, however, **2** had transformed completely into **3** proving that **2** is sensitive towards water (humidity).

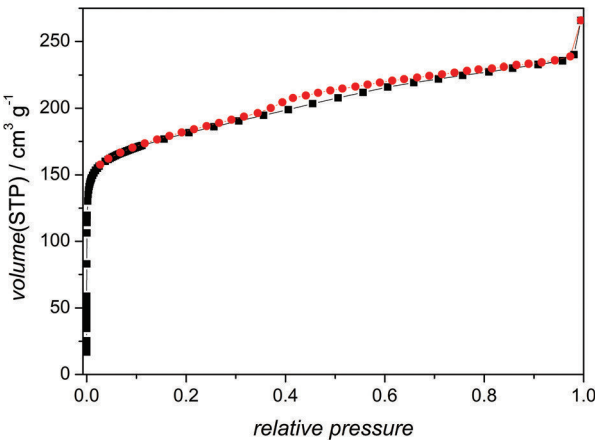

Fig. 11 MC-**2**: Ar adsorption (black) and desorption (red) isotherms measured at −186 °C.

Investigation of energy landscape

Up to now no more than two polymorphs had been reported for Zn-based ZIFs containing 4,5-disubstituted imidazolate linkers. Our experimental work above has now revealed that the [Zn(dcim)$_2$] system is at least trimorphic, possibly implying a more rich polymorphism of such ZIF systems. To get an impression of possible structures, we investigated the relative stabilities of ZIFs **1**–**3** and looked for further hypothetical polymorphs as was done in our previous work.[9,26] The calculations were performed with the recently developed rVV10 DFT functional[27] that accounts fairly well for the van der Waals interactions.

The energy landscape of the [Zn(dcim)$_2$] system is displayed in Fig. 12 in the form of an energy–density diagram. It can be seen that the experimental polymorphs **1** (RHO) and **2** (SOD,

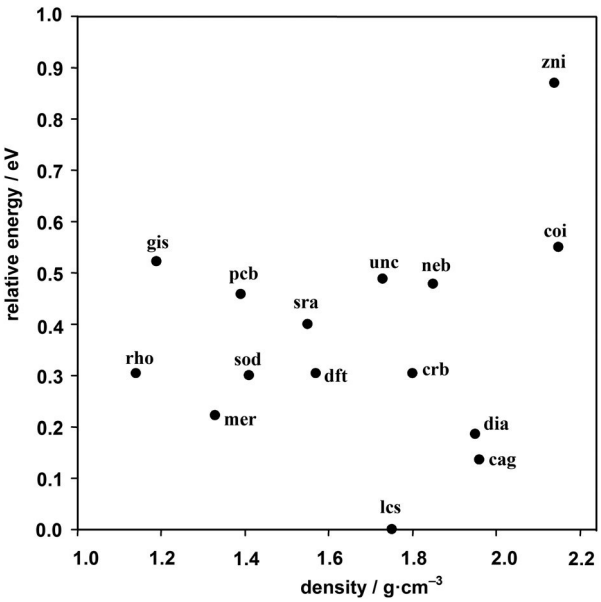

Fig. 12 Energy-density diagram of the energy landscape for the [Zn(dcim)$_2$] system.

framework **I**) are nearly isoenergetic, whereas **3** (lcs) represents the ground state (among the topologies considered) and is stabilised by ~25 kJ mol^{-1}. Considering desirable low-density (porous) frameworks it is of interest that MER and DFT have energies close to RHO and SOD. Similar trends for porous networks were observed earlier for the $[Zn(im)_2]$ and $[Zn(2\text{-}mim)_2]$ systems.[9,26] The calculated energy landscape thus supports the idea that more porous polymorphs might be synthetically accessible in this ZIF system. Additionally, we note that dense framework types (*e.g.* zni and coi) become unfavourable due to short inter-linker Cl···Cl distances. It should be emphasised that our total energy calculations do not include finite temperature effects and entropic contributions as well as the influence of solvent/guest molecules.

The role of solvents in crystallisation processes[19b,28] can likely explain our synthetic results presented above, *i.e.* the fact that we obtained **2** in the form of framework **II** rather than **I**.

Conclusions

We reported a rapid additive-free synthesis of NCs of RHO-type ZIF-71 (**1**) with very small size, large porosity and good thermal as well as chemical stability and the solution mediated phase transformation of NC-**1** into a novel polymorph (**2**) with SOD topology which in turn converts into lcs-type ZIF-72 (**3**). MC-**2** and NC-**2** were synthesised *via* coordination modulation and a solvent assisted ligand exchange-related process, respectively. DFT-assisted Rietveld analysis of powder XRD data was utilised for a first determination of the crystal structure of **2** which exhibits an unusual SOD framework conformation with cubic symmetry. The different materials of **2** obtained *via* the various synthetic methods exhibit structural variability with lower than cubic symmetry. Novel **2** is microporous but less stable towards water (humidity) than NC-**1**. Our experimental studies revealed for the first time that Zn-based ZIFs containing 4,5-disubstituted imidazolate linkers can be at least trimorphic and DFT calculations predict that further as-yet unknown microporous polymorphs might be synthetically accessible in the $[Zn(dcim)_2]$ system.

Experimental section

Materials and methods of characterisation

All starting materials were used as received from the commercial supplier Sigma-Aldrich.

Powder XRD patterns were recorded at room temperature using a Stoe STADI-P transmission diffractometer equipped with a linear position sensitive detector and a curved Ge(111) monochromator providing $CuK_{\alpha1}$ radiation. VT-XRD experiments were performed on a Stoe STADI-P diffractometer equipped with a Stoe high temperature oven in the Debye–Scherrer mode ($CuK_{\alpha1}$ radiation). Samples were kept in unsealed, thin-walled silica glass capillaries with an outer diameter of 0.5 mm. TGA and difference thermal analysis (DTA) were performed simultaneously on a Netzsch 429 thermoanalyser. Samples were filled in alumina crucibles and heated in a flow of air with a heating ramp of 5 K min^{-1} from room temperature up to 1000 °C. For Ar physisorption experiments at −186 °C a Quantachrome Autosorb1-MP volumetric apparatus was used. Samples were degassed in a dynamic vacuum at 100 °C for at least 3 d before starting the measurements. Afterwards XRD patterns were recorded to check that the ZIF frameworks had withstood the activation procedures. Surface areas were estimated applying the BET equation within the range $0.03 < p/p_0 < 0.08$. Micropore volumes were obtained at a single point. SEM images were taken on a Jeol JSM-6700F instrument with a field emitter as the electron source. A low acceleration voltage (2 kV), a low current (10 μA) and a lens distance of 3–8 mm were used. Time-resolved *in situ* SLS experiments were performed at 25 °C on a home-built multi-angle goniometer using cylindrical silica glass cuvettes. Each time-resolved experiment was initiated by filtering 3 mL of 1-propanolic $Zn(NO_3)_2{\cdot}6H_2O$ and 3 mL of 1-propanolic Hdcim solutions into the cuvette whereby addition of the second component solution defined time zero. The scattering curves were approximated by means of a Guinier fit to extract the accumulated weight-averaged molar mass of the growing particles. The instrument as well as general experimental and data evaluation procedures are described elsewhere.[12b]

Synthesis of NC-1

NC-**1** was synthesised at room temperature by pouring a solution of 1465.9 mg (10.702 mmol) Hdcim in 100 mL 1-PrOH into a solution of 795.9 mg (2.676 mmol) $Zn(NO_3)_2{\cdot}6H_2O$ in 100 mL 1-PrOH. The mixture was stirred for 5 min and the NCs were collected by centrifugation at 10 000*g* for 5 min. The obtained colourless NCs were dispersed in 200 mL of EtOH by using an ultrasonic finger and separated by centrifugation at 10 000*g* for 60 min. The product was dried in air at room temperature. The yield was 12% based on Zn.

Synthesis of MC-2 *via* modulated synthesis used for general characterisation

MC-**2** was obtained at room temperature by pouring a solution of 732.9 mg (5.351 mmol) Hdcim and 427 μL (5.351 mmol) 1-mim in 50 mL 1-PrOH into a solution of 398.0 mg (1.338 mmol) $Zn(NO_3)_2{\cdot}6H_2O$ in 50 mL 1-PrOH under stirring. Stirring was continued for 24 h. The solid was separated by centrifugation and washed with EtOH. Two centrifugation/washing cycles were applied. The product was dried in air at room temperature. The yield was 71% based on Zn.

Synthesis of big crystals of 2 *via* modulated synthesis

Typically, 79.2 mg (0.266 mmol) $Zn(NO_3)_2{\cdot}6H_2O$ were dissolved in 10 mL 1-PrOH. A second solution was prepared by dissolving 145.9 mg (1.065 mmol) Hdcim and 84.9 μL (1.065 mmol) 1-mim in 10 mL 1-PrOH. The latter solution was poured into the former solution under stirring. Stirring was stopped and the closed glass tube was heated at 50 °C in a convection oven

for 24 h. The rhombic dodecahedral crystals (up to 100 μm in size) were filtered and washed with 1-PrOH.

Synthesis of NC-2 *via* a solvent assisted ligand exchange-related process

The NC-ZIF-8 template material was synthesised as described elsewhere.[7c] For SALE 50 mg (0.022 mmol) of activated NC-ZIF-8 were dispersed in 20 mL of 1-PrOH containing 150.5 mg (1.099 mmol) of Hdcim by sonication. The closed glass tube was heated at 100 °C in a convection oven for 5 d. Every 24 h the solid was centrifuged, washed with 1-PrOH and redispersed in a fresh 1-propanolic solution of the same Hdcim concentration. The final product was dried at 50 °C.

The degree of ligand exchange was checked by ^{1}H-NMR. About 30 mg of solid were digested in a mixture of 500 μL of 35 wt% DCl and 250 μL of D_2O.

Structure analysis of 2

Powder XRD data with a good signal-to-noise ratio were recorded at room temperature on a Stoe STADI-P diffractometer in Debye–Scherrer geometry using $CuK_{\alpha1}$ radiation (λ = 1.540596 Å) and a linear position sensitive detector. Activated material prepared by SALE was filled in thin-walled borosilicate glass capillaries with an outer diameter of 0.3 mm. The intensity profiles were scanned between $5° \leq 2\theta \leq 50°$ in steps of 0.1° 2θ with a recording time of 130 s per step (internal detector resolution 0.01° 2θ). Indexing, Pawley refinement and Rietveld refinement were performed using TOPAS software.[29] Intensity profiles were modelled with modified Thompson–Cox–Hastings pseudo-Voigt peak-shape and Chebychev background functions. A simple axial model was applied to treat peak anisotropy. The dcim unit was treated as a rigid body allowing twisting about a Zn⋯Zn edge during all refinements. Initially applied restraints on Zn–N bond lengths and N–Zn–N angles were completely released in the final cycles of refinement. Two isotropic displacement parameters (Zn atom, linker atoms) were refined.

Crystal data for desolvated framework **II**: $C_6H_2Cl_2N_4Zn$, M = 337.311 g mol^{-1}, cubic, $I\bar{4}3m$, a = 16.8179(16) Å, U = 4756.8(14) Å^3, Z = 12, D_c = 1.413 g cm^{-3}, T = 24 °C, R_p = 5.297, R_{wp} = 7.979, R_{exp} = 2.669, GOF = 2.989, R_{Bragg} = 7.579. Atomic parameters, bond lengths and bond angles are listed in Tables S1–S3,† respectively. Full crystallographic data are provided in CIF format in the ESI.†

DFT calculations

DFT calculations were performed with the rVV10 DFT functional as implemented in the PWscf/Quantum ESPRESSO package.[30] The Kohn–Sham equations (without spin polarisation) were solved using the plane-wave pseudopotential approach (ultrasoft pseudopotentials were used). A kinetic energy cutoff of 80 Ry and a density cutoff of 460 Ry were used to achieve fully converged results. During structure relaxation, the atomic positions and unit cell parameters were optimised. In the optimised structures the residual forces were smaller than 0.02 eV Å^{-1} and the pressure converged within 0.1 GPa. In most structures (with the cell parameter >15.0 Å), Γ-point approximation was sufficient to achieve the convergence while in the structures with smaller cells a standard Monkhorst–Pack k-mesh (at most 2 × 2 × 2) was employed for the summation over the Brillouin zone. Data for all optimised ZIF framework structures are provided in CIF format in the ESI.†

Acknowledgements

The authors are grateful to Natalja Wendt and Jann Lippke for performing gas sorption analyses, Dr Jörg Fohrer for recording NMR spectra and Uta Sazama for measuring TG/MS data. Financial support by the DFG (Priority Program 1415 "Crystalline Non-equilibrium Phases") is gratefully acknowledged.

Notes and references

1 (*a*) A. Phan, C. J. Doonan, F. J. Uribe-Romo, C. B. Knobler, M. O'Keeffe and O. M. Yaghi, *Acc. Chem. Res.*, 2010, **43**, 58; (*b*) J.-P. Zhang, Y.-B. Zhang, J.-B. Lin and X.-M. Chen, *Chem. Rev.*, 2012, **112**, 1001.

2 (*a*) K. S. Park, Z. Ni, A. P. Côté, J. Y. Choi, R. Huang, F. J. Uribe-Romo, H. K. Chae, M. O'Keeffe and O. M. Yaghi, *Proc. Natl. Acad. Sci. U. S. A.*, 2006, **103**, 10186; (*b*) X.-C. Huang, Y.-Y. Lin, J.-P. Zhang and X.-M. Chen, *Angew. Chem., Int. Ed.*, 2006, **45**, 1557.

3 R. Banerjee, A. Phan, B. Wang, C. Knobler, H. Furukawa, M. O'Keeffe and O. M. Yaghi, *Science*, 2008, **319**, 939.

4 (*a*) H. Bux, F. Liang, Y. Li, J. Cravillon, M. Wiebcke and J. Caro, *J. Am. Chem. Soc.*, 2009, **131**, 16000; (*b*) K. Li, D. H. Olson, J. Seidel, T. J. Emge, H. Gong, H. Zeng and J. Li, *J. Am. Chem. Soc.*, 2009, **131**, 10368.

5 C. Chizallet, S. Lazare, D. Bazer-Bachi, F. Bonnier, V. Lecocq, E. Soyer, A.-A. Quoineaud and N. Bats, *J. Am. Chem. Soc.*, 2010, **132**, 12365.

6 (*a*) G. Lu and J. T. Hupp, *J. Am. Chem. Soc.*, 2010, **132**, 7832; (*b*) T. T. Isimjan, H. Kazemian, S. Rohani and A. K. Ray, *J. Mater. Chem.*, 2010, **20**, 10241; (*c*) S. B. Kalidindi, D. Esken and R. A. Fischer, *Chem.–Eur. J.*, 2011, **17**, 6594; (*d*) S. Ma, G. A. Goenaga, A. V. Call and D.-J. Liu, *Chem.–Eur. J.*, 2011, **17**, 2063; (*e*) C.-Y. Sun, C. Qin, X.-L. Wang, G.-S. Yang, K.-Z. Shao, Y.-Q. Lan, Z.-M. Su, P. Huang, C.-G. Wang and E.-B. Wang, *Dalton Trans.*, 2012, **41**, 6906.

7 (*a*) J. Cravillon, S. Münzer, S.-J. Lohmeier, A. Feldhoff, K. Huber and M. Wiebcke, *Chem. Mater.*, 2009, **21**, 1410; (*b*) Y.-S. Li, H. Bux, A. Feldhoff, G.-L. Li, W.-S. Yang and J. Caro, *Adv. Mater.*, 2010, **22**, 3322; (*c*) J. Cravillon, R. Nayuk, S. Springer, A. Feldhoff, K. Huber and M. Wiebcke, *Chem. Mater.*, 2011, **23**, 2130.

8 (*a*) Y. Phan, Y. Liu, G. Zeng, L. Zhao and Z. Lai, *Chem. Commun.*, 2011, **47**, 2071; (*b*) Y. Phan, D. Heryadi, F. Zhou, L. Zhao, G. Lestari, H. Su and Z. Lai, *CrystEngComm*, 2011, **13**, 6937; (*c*) S. Tanaka, K. Kida, M. Okita, Y. Ito and Y. Miyake, *Chem. Lett.*, 2012, **41**, 1337.

9 I. A. Baburin, S. Leoni and G. Seifert, *J. Phys. Chem. B*, 2008, **112**, 9437.
10 (*a*) P. J. Beldon, L. Fábián, R. S. Stein, A. Thirumurugan, A. K. Cheetham and T. Friscic, *Angew. Chem., Int. Ed.*, 2010, **49**, 9640; (*b*) M. Lanchas, D. Vallejo-Sánchez, G. Beobide, O. Castillo, A. T. Aguayo and P. Román, *Chem. Commun.*, 2012, **48**, 9930.
11 (*a*) O. Karagiaridi, M. B. Lalonde, W. Bury, A. A. Sarjeant, O. K. Farha and J. T. Hupp, *J. Am. Chem. Soc.*, 2012, **134**, 18790; (*b*) H. Fei, J. F. Cahill, K. A. Prather and S. M. Cohen, *Inorg. Chem.*, 2013, **52**, 4011; (*c*) O. Karagiaridi, W. Bury, A. A. Sarjeant, C. L. Stern, O. K. Farha and J. T. Hupp, *Chem. Sci.*, 2012, **3**, 3256.
12 (*a*) J. Cravillon, C. A. Schröder, R. Nayuk, J. Gummel, K. Huber and M. Wiebcke, *Angew. Chem., Int. Ed.*, 2011, **50**, 8067; (*b*) T. Hikov, C. A. Schröder, J. Cravillon, M. Wiebcke and K. Huber, *Phys. Chem. Chem. Phys.*, 2012, **4**, 511; (*c*) T. Friscic, I. Halasz, P. J. Beldon, A. M. Belenguer, F. Adams, S. A. J. Kimber, V. Honkimäki and R. E. Dinnebier, *Nat. Chem.*, 2013, **5**, 66; (*d*) M. Goesten, E. Stavitski, E. A. Pidko, C. Gücüyener, B. Boshuizen, S. N. Ehrlich, E. J. M. Hensen, F. Kapteijn and J. Gascon, *Chem.–Eur. J.*, 2013, **19**, 7809; (*e*) P. Cubillas, M. W. Anderson and M. P. Attfield, *Chem.–Eur. J.*, 2013, **19**, 8236.
13 W. Morris, B. Leung, H. Furukawa, O. K. Yaghi, N. He, H. Hayashi, Y. Houndonougbo, M. Asta, B. B. Laird and O. M. Yaghi, *J. Am. Chem. Soc.*, 2010, **132**, 11006.
14 (*a*) A. Nalaparaju, X. S. Zhao and J. W. Jiang, *J. Phys. Chem. C*, 2010, **114**, 11542; (*b*) A. Nalaparaju and J. Jiang, *Langmuir*, 2012, **28**, 15305.
15 (*a*) R. P. Lively, M. E. Dose, J. A. Thompson, B. A. McCool, R. R. Chance and W. J. Koros, *Chem. Commun.*, 2011, **47**, 8667; (*b*) K. Zhang, R. P. Lively, M. E. Dose, A. J. Brown, C. Zhang, J. Chung, S. Nair, W. J. Koros and R. R. Chance, *Chem. Commun.*, 2013, **49**, 3245.
16 (*a*) X. Dong and Y. S. Lin, *Chem. Commun.*, 2013, **49**, 1196; (*b*) S. Liu, G. Liu, X. Zhao and W. Jin, *J. Membr. Sci.*, 2013, **446**, 181.
17 (*a*) T. Tsuruoka, S. Furukawa, Y. Takashima, K. Yoshida, S. Isoda and S. Kitagawa, *Angew. Chem., Int. Ed.*, 2009, **48**, 4739; (*b*) A. Schaate, P. Roy, A. Godt, J. Lippke, F. Waltz, M. Wiebcke and P. Behrens, *Chem.–Eur. J.*, 2011, **17**, 6643.
18 J. T. Hughes, T. D. Bennett, A. K. Cheetham and A. Navrotsky, *J. Am. Chem. Soc.*, 2013, **135**, 598.
19 (*a*) Y.-Q. Tian, L. Xu, C.-X. Cai, J.-C. Wei, Y.-Z. Li and X.-Z. You, *Eur. J. Inorg. Chem.*, 2004, 1039; (*b*) Y.-Q. Tian, Y.-M. Zhao, Z.-X. Chen, G.-N. Zhang, L.-H. Weng and D.-Y. Zhao, *Chem.–Eur. J.*, 2007, **13**, 4146; (*c*) C. A. Schröder, I. A. Baburin, L. van Wüllen, M. Wiebcke and S. Leoni, *CrystEngComm*, 2013, **15**, 4036.
20 B. P. Biswal, T. Panda and R. Banerjee, *Chem. Commun.*, 2012, **48**, 11868.
21 J. Cravillon, C. A. Schröder, H. Bux, A. Rothkirch, J. Caro and M. Wiebcke, *CrystEngComm*, 2012, **14**, 492.
22 M. O'Keeffe, M. A. Peskov, S. J. Ramsden and O. M. Yaghi, *Acc. Chem. Res.*, 2008, **41**, 1782.
23 (*a*) W. Morris, C. J. Doonan, H. Furukawa, R. Banerjee and O. M. Yaghi, *J. Am. Chem. Soc.*, 2008, **130**, 12626; (*b*) S. A. Moggach, T. D. Bennett and A. K. Cheetham, *Angew. Chem., Int. Ed.*, 2009, **48**, 7087.
24 A. L. Spek, *J. Appl. Crystallogr.*, 2003, **36**, 7.
25 (*a*) S. Aguado, C.-H. Nicolas, V. Moizan-Baslé, C. Nieto, H. Amrouche, N. Bats, N. Audebrand and D. Farrusseng, *New J. Chem.*, 2011, **35**, 41; (*b*) W. Morris, N. He, K. G. Ray, P. Klonowski, H. Furukawa, I. N. Daniels, Y. A. Houndonougbo, M. Asta, O. M. Yaghi and B. B. Laird, *J. Phys. Chem. C*, 2012, **116**, 24084.
26 (*a*) I. A. Baburin and S. Leoni, *J. Mater. Chem.*, 2012, **22**, 10152; (*b*) I. A. Baburin, A. Assfour, G. Seigert and S. Leoni, *Dalton Trans.*, 2011, **40**, 3796.
27 R. Sabatini, T. Gorni and S. de Gironcoli, *Phys. Rev. B: Condens. Matter*, 2013, **87**, 041108.
28 J.-P. Zhang, X.-C. Huang and X.-M. Chen, *Chem. Soc. Rev.*, 2009, **38**, 2385.
29 TOPAS, *Bruker AXS GmbH*, Karlsruhe, Germany, 2009.
30 http://www.quantum-espresso.org

